JOURNAL OF SOLID STATE CHEMISTRY **128,** 1–16 (1997)
ARTICLE NO. SC967092

Valence Stabilization, Mixed Crystal Chemistry, and Electronic Transitions in Tetrahedral Oxo and Hydroxo Cr(IV), Mn(V), and Fe(VI) Clusters: A Theoretic Investigation

M. Atanasov[1]

Institute of General and Inorganic Chemistry, Bulgarian Academy of Sciences, Bl. 11, Sofia 1113, Bulgaria

and

H. Adamsky and K. Eifert

Institut für Theoretische Chemie, Heinrich-Heine Universität, Universitätsstr.1, Geb.26.32, Düsseldorf, D-40225, Germany

Received March 26, 1996; in revised form June 27, 1996; accepted July 9, 1996

Ab initio **Hartree–Fock SCF (HF-SCF) and multiconfiguration complete active space SCF (CASSCF) calculations have been carried out on tetrahedral $M(OH)_4^z$ and $MO_4^{z'}$ model clusters (M, z, z': Cr^{IV}, 0, −4; Mn^V, 1, −3; Fe^{VI}, 2, −2) in their $^3A_2$ ground state and in selected triplet and singlet ligand field and charge transfer excited states. Ground state orbital energies and charge distributions supplemented with calculations using a semiempirical approach (Jørgensen) help characterize the stabilization of Cr^{IV}, Mn^V, and Fe^{VI} in terms of competing ionic and covalent forces. The crucial role of the Madelung energy in stabilizing these unusual oxidation states is emphasized. Frozen orbitals as obtained by state averaging over d^2 triplet and singlet states are used to compare results from Hartree–Fock and ligand field treatments. Calculations using these orbitals show that interelectronic repulsion parameters in tetra-oxo coordinated Cr^{IV}, Mn^V, and Fe^{VI} are considerably reduced compared to their free ionic values. Charge transfer states are found to further modify energy levels of d^2 type, leading to an effective lowering of Coulomb repulsion parameters in the order of the e^2, $e^1t_2^1$, and t_2^2 strong field configurations. Theories of isomorphic substitution for ionic solids are not applicable for the systems under consideration. Comparison between available structural and spectral data shows that Cr^{IV}, Mn^V, and Fe^{VI} ions in dilute mixed crystals with isovalent tetrahedral host ions, such as Si^{IV}, P^V, and S^{VI}, assume geometries close to those known for stoichiometric phases with CrO_4^{4-}, MnO_4^{3-}, and FeO_4^{2-} tetrahedra. Covalent contributions to the lattice energy from guest (d^2) and host tetrahedra are additive, and mixing enthalpies are small or negligible, allowing for continuous solid solutions even when guest and host ions, such as Mn^V and P^V, Fe^{VI} and S^{VI}, differ considerably in their size.**

[1] To whom correspondence should be addressed at the Institute für Theoretische Chemie, Heinrich-Heine Universität, Universitätsstrasse 1, Geb.26.32, D-40225 Düsseldorf, Germany.

I. INTRODUCTION

Isoelectronic d^2 cations Cr^{IV}, Mn^V, and Fe^{VI} in various oxide ceramics have been subject to extensive studies, both experimental and theoretical, because of their remarkable luminescence properties (1–12) and applications, in the case of Cr^{IV}, in tunable lasers in the near infrared (13–16). The oxidation states of tetrahedrally coordinated Cr^{IV}, Mn^V, and Fe^{VI} ions are rather unstable when compared to those of Cr^{III}, Cr^{VI}, Mn^{II}, Mn^{III}, Mn^{IV}, Mn^{VII}, and Fe^{III}. From a formal point of view the oxidation state can be unambiguously attributed to a given preponderant ground state electronic configuration which for tetrahedrally coordinated d^2 metals consists of two unpaired electrons in the antibonding e orbital [$^3A_2(e^2)$-ground state] and fully occupied bonding (a_1, e, and t_2) and nonbonding ligand (t_1, t_2) orbitals. While orbital contributions from ligand (2s, 2p) and metal (3d) functions to the highest occupied molecular orbitals of e symmetry may vary in a wide range for a given electronic configuration, transfer of electrons from a nonbonding ligand, t_1 and t_2, to antibonding metal e and t_2 orbitals (usually encountered as charge transfer bands in the optical spectra for species in stable oxidation states) may take place in the ground state and break the valence form. Preparation and characterization of Cr^{IV}, Mn^V, and Fe^{VI} valence forms in solids present a real challenge for inorganic chemists (17). It is therefore of fundamental interest to study the factors that affect the stabilization of these oxidation states when the respective cations isomorphically substitute, such as Ge^{IV}, Si^{IV} (Cr^{IV}), P^V, As^V, V^V, (Mn^V), and S^{VI}, Cr^{VI}, Se^{VI} (Fe^{VI}), and further how the character of metal–ligand bonding changes from left to right in the 3d transition metal isoelectronic (d^2) series. In an attempt to contribute to the solution of these problems we have performed Hartree–

0022-4596/97 $25.00

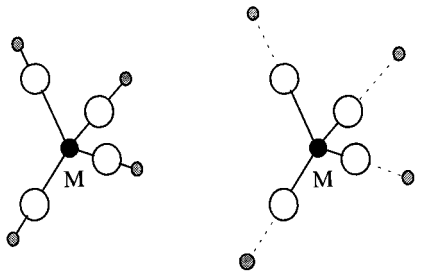

FIG. 1. Model clusters for *ab initio* calculations: $M(OH)_4^{z}$ (left) and $MO_4^{z'} \cdot 4H^+$ (right).

Fock SCF and complete active space SCF (CASSCF) calculations, as well as an analysis using a semiempirical approach (18), on isoelectronic Cr^{IV}, Mn^{V}, and Fe^{VI} in tetrahedral coordination with O^{2-} or OH^- ions (Fig. 1). These are used here as cluster models for color centers in oxidic matrices and molecular complexes, respectively. In the oxo clusters we have introduced four bare protons behind the metal–oxygen bonds in order to simulate the Madelung field and to counterbalance the excess negative charges.

d^2 cations in tetrahedral coordination assume strong field configurations e^2, $e^1t_2{}^1$, and $t_2{}^2$ and give rise to a triplet ground state ($^3A_2(e^2)$) and $^3T_2(e^1t_2{}^1)$, $_a{}^3T_1(e^1t_2{}^1)$, $_b{}^3T_1(t_2{}^2)$, $^1E(e^2)$, and $^1A_1(e^2)$ excited states. Higher energy singlet states will not be discussed here but they are taken into account explicitly in the CASSCF calculations, thus influencing the singlets of the ground state configuration via nondiagonal elements. d–d transitions of low valent $3d$ cations in cubic fields are known to be adequately described by classical ligand field theory with ligand field strength $10Dq$ given by the energy difference $E[^3T_2(e^1t_2{}^1)] - E[^3A_2(e^2)]$ and with Racah parameters B and C for the interelectronic repulsion, the C/B ratio being approximately identical with the free ion C_o/B_o value. B is reduced due to metal–ligand overlap with respect to the free ion value B_o ($\beta = B/B_o < 1$). In the case of covalent bonds, a more sophisticated approach proposed by C. E. Schäffer and C. K. Jørgensen (19, 20) was found to be more adequate. Here, different B values, B_{ee}, B_{et}, and B_{tt}, are introduced for the e^2, $e^1t_2{}^1$, and $t_2{}^2$ electron configurations, respectively (Eq. [1]), implying a more pronounced covalency for electrons occupying t_2, compared to e orbitals ($t' < e' < 1$) (21):

$$\begin{aligned} B_{ee} &= e'^4 B_o \\ B_{et} &= e'^2 t'^2 B_o \\ B_{tt} &= t'^4 B_o . \end{aligned} \qquad [1]$$

Optical transitions reported for $CrO_4{}^{4-}$ could be fitted nicely with $10Dq$ and two nephelauxetic reduction factors e' and t' [Eq. [1]] in the case of Cr^{IV} (4, 17). Switching to Mn^{V}, the energies of the spin-forbidden transitions $^3A_2 \rightarrow {}^1E$, $^1A_1$ can be reproduced by B_{ee} (and $C_{ee} = 4.25\,B_{ee}$) only within about $500\ cm^{-1}$. In the case of Fe^{VI} even the Jørgensen treatment breaks down due to low-lying ligand-to-metal charge transfer bands, extending down to $17{,}700\ cm^{-1}$ into the visible region (12). They interact with the energetically neighbored d–d transitions, leading to a more pronounced admixture of ligand orbitals into the mainly $3d$ wavefunctions and an energetic depression of the respective d–d bands. Since the $^1A_1$ state lies much higher in energy than the ^1E, it is affected much more strongly, in accordance with experiment. In order to describe the electronic states in the limit of extensive mixing of ligand field and charge transfer states a method more general than ligand field theory is needed. Recently, a configuration interaction model has been applied (22) in which ligand-to-metal charge transfer (Δ) and metal–ligand coupling (t), in addition to the usual crystal field treatment with $10Dq$ and nonreduced free ion B and C parameters, have been taken into account, making it possible to analyze intermixing of $d^3\underline{L}$-charge transfer states ($\underline{L}$-hole on the ligands) into the d^2-ionic multiplets more closely. The decrease of Δ in the order Cr^{IV}, Mn^{V}, Fe^{VI}

TABLE 1
^3F and ^3P Energies, Coulomb Repulsion Parameters J and X (in a.u.), and Calculated Racah Parameters A, B, and C (in cm^{-1}) of the Isoelectronic Free Cr^{4+}, Mn^{5+}, and Fe^{6+} Ions Calculated Using HF-SCF(3-21G) and Average Triplet Orbitals[a]

	Cr^{4+}	Mn^{5+}	Fe^{6+}
$E(^3F)$	− 1039.679416	− 1143.383631	− 1252.221510
$E(^3P)$	− 1039.592657	− 1143.285933	− 1252.113927
$E(^3P) - E(^3F) = 15B$	0.086759	0.097698	0.113927
$J = 25A + 35C$	22.531713	25.128078	27.472513
$X = 5A + 70B + 35C$	5.524613	6.176763	6.765747
A	191,059	212,952	232,721
B	1269 (1015)	1429 (1160)	1574 (1300)
C	4808 (4263)	5449 (4930)	6029 (5525)

[a] Values in parentheses refer to B and C deduced from atomic spectral data (21).

TABLE 2

HF-SCF–Orbital Energies (in a.u., TZV-basis sets), Metal Orbital Percentages of Each *MO* (in Parentheses), and Interatomic Distances (in Å) from Geometry Optimizations on Tetrahedral Oxo and Hydroxo Model Clusters of Cr^{IV}, Mn^{V}, and Fe^{VI} in Their $^3A_2(2e^2)$ States

Model cluster	$Cr(OH)_4$	$CrO_4^{4-}\cdot 4H^+$	$Mn(OH)_4^+$	$MnO_4^{3-}\cdot 4H^+$	$Fe(OH)_4$	$FeO_4^{2-}\cdot 4H^+$
M–O bond length	1.730	1.766	1.628	1.660	1.623	1.609
O–H bond length[a]	0.937	2.000	0.951	2.000	0.975	2.000
$2e$	− 0.2497(90.9)	0.0134(92.5)	− 0.5592(80.8)	− 0.2512(87.1)	− 0.8194(19.2)	− 0.5115(84.7)
$1t_1$	− 0.4502(0)	− 0.1994(0)	− 0.6743(0)	− 0.4072(0)	− 0.8064(0)	− 0.6419(0)
$3t_2$	− 0.5095(8.8)	− 0.2569(4.0)	− 0.7640(13.8)	− 0.4785(3.4)	− 0.9174(15.9)	− 0.7126(5.0)
$1e$	− 0.5097(10.0)	− 0.2575(8.4)	− 0.7656(22.6)	− 0.4872(15.3)	− 1.1730(83.9)	− 0.7315(19.6)
$2t_2$	− 0.7009(13.3)	− 0.3026(16.1)	− 0.9754(21.1)	− 0.5537(32.9)	− 1.2223(19.0)	− 0.8272(49.2)
$2a_1$	− 0.7162(2.8)	− 0.3052(18.6)	− 0.9711(2.8)	− 0.5151(16.3)	− 1.2201(3.7)	− 0.7240(10.9)
$1t_2$	− 1.2867(4.4)	− 0.9702(8.2)	− 1.5345(5.9)	− 1.2008(9.1)	− 1.7441(5.0)	− 1.4487(9.6)
$1a_1$	− 1.3013(1.2)	− 0.9897(9.2)	− 1.5543(1.5)	− 1.2256(9.4)	− 1.7628(1.9)	− 1.4750(8.2)
$\Delta E(2e - 1t_1)$	0.2005	0.2128	0.1151	0.1560	0.0130	0.1304
$\Delta E(1t_1 - 1e)$	0.0595	0.0581	0.0913	0.0800	0.3666	0.0896
$\Delta E(1t_1 - 2t_2)$	0.2507	0.1032	0.3011	0.1465	0.4159	0.1853
$\Delta E(1t_1 - 2a_1)$	0.2660	0.1058	0.2968	0.1079	0.4137	0.0821
σ_L	0.1732	0.0629	0.2030	0.0899	0.2203	0.1166
π_L	0.0223	0.0218	0.0342	0.0300	0.1375	0.0336
$\sigma(4s)$	0.0665	0.0264	0.0742	0.0270	0.1034	0.0205
π_L/σ_L	0.129	0.346	0.168	0.334	0.624	0.288
E_t	− 1345.1200	− 1343.7467	− 1451.0484	− 1449.9818	− 1562.8676	− 1562.1513

[a] O–H bond lengths in hydroxo clusters are optimized, those for oxo anions are held fixed at 2 Å. Notations: σ_L, $\sigma(4s)$, and π_L orbital bonding parameters of σ and π type, E_t-$^3A_2$ HF-SCF-total energies.

results in an effective lowering in electronic repulsion and variable *B* and *C* values even for terms stemming from the same strong field electronic configuration such as $^3A_2(e^2)$, $^1E(e^2)$, and $^1A_1(e^2)$. The extent of mixing of d^2 and $d^3\underline{L}$ configurations and the involved covalency were found to increase in the order $^3A_2$, ^1E, $^1A_1$. This effect is weak for Cr^{IV}, more pronounced for Mn^{V}, and rather strong for Fe^{VI}. In the present work we will analyze these effects in terms of first-principles calculations. Comparing HF-SCF with CASSCF energies will help to specify more precisely the limits of application of ligand field descriptions based on orbital and Coulomb repulsion parameters common for all multiplets. The roles of ionic and covalent bonding in stablizing these unusual oxidation states are analyzed.

II. *AB INITIO* CALCULATIONS

All calculations in this work were performed using the *ab initio* program GAMESS, developed by Schmidt *et al.* (23), using 3-21G (24, 25) and TZV (26) (modified Wachters' orbitals $14s11p6d/10s8p3d$ for Cr, Mn, and Fe (26), $11s6p/5s3p$ for O, and $5s/3s$ for H) basis sets. Cr^{IV}, Mn^{V}, and Fe^{VI} free ions in their ground ^3F and excited ^3P d^2 states and Colomb repulsion parameters were calculated using the multiconfiguration SCF (MCSCF) option of the program and the common set of orbitals achieved by averaging the second-order density matrix over all 10 configuration state functions (CSF). ^3F and ^3P state energies are listed in Table 1. Restricted open shell HF (ROHF) calculations on oxo $[MO_4^z\cdot 4H^+$ (*M*, *z*: Cr(IV), $z = -4$; Mn(V), $z = -3$; Fe(VI), $z = -2]$ and hydroxo $[M(OH)_4^z$ (*M*, *z*: Cr(IV), $z = 0$; Mn(V), $z = +1$; Fe(VI), $z = +2]$ clusters (Fig. 1) in their $^3A_2(e^2)$ states are performed, imposing linear *M*–O–H and *M*–O^- H^+ moieties for $M(OH)_4^z$ and $MO_4^z\cdot 4H^+$, respectively.[2] Optimized *M*–O bond distances, orbital energies, corresponding metal orbital percentages for each *MO*, and, for $M(OH)_4^z$, the O–H bond distance are listed in Table 2. Ground state ($^1A_1$) HF-SCF calculations have been also performed for tetrahedral $M^{IV}(SiO_4^{4-}, GeO_4^{4-})$, $M^{V}(VO_4^{3-}, PO_4^{3-})$, and $M^{VI}(FeO_4^{2-}, SO_4^{2-}, CrO_4^{2-})$ ions serving as host sites to stabilize Cr^{IV}, Mn^{V}, and Fe^{VI}, respectively. Bond distances, atomic charges, and bond orders for all these oxo anions are listed in Table 3. Optimized bond distances were adopted without changes for all excited d^2 and ligand-to-metal charge transfer states of Cr^{IV}, Mn^{V}, and Fe^{VI}. $O^{2-}\cdots H^+$ distances for $MO_4^z\cdot 4H^+$ clusters were fixed at an arbitrary distance of 2 Å, which approximately matches O^{2-}–counterion (M^{II}) separations in oxidic host lattices. Optimized bond lengths for $M(OH)_4^z$ obtained with TZV-basis sets (Table 2) have been further

[2] Optimized *M*–O–H geometries become nonlinear when treating *M*–O–H angles as variable parameters. The resulting optimized geometries for $M(OH)_4$ are of D_{2d} type. This result is not relevant for this study; however, it can help elucidate the effect of ligand lone pairs and bent bonds on the *d* multiplets in coordination compounds.

TABLE 3

Optimized M–O Bond Distances (Å), Atomic Charges, Bond Orders, Harmonic Force Field Parameters ($cm^{-1}/Å^2$), and Calculated vs Experimental Stretching Mode Fundamentals (cm^{-1}) for Tetra-Oxo Anions of Cr^{IV}, Mn^{V}, and Fe^{VI} and Corresponding Host Ions Ge^{IV}, Si^{IV}, P^{V}, S^{V}, and Cr^{VI} as Obtained from HF-SCF Calculations on Tetrahedral $MO_4^{z} \cdot 4H^+$ Model Clusters Using TZV in All Cases Except for $GeO_4^{4-} \cdot 4H^+$ (DZV basis)

	$CrO_4^{4-} \cdot 4H^+$	$GeO_4^{4-} \cdot 4H^+$	$SiO_4^{4-} \cdot 4H^+$	$MnO_4^{3-} \cdot 4H^+$	$VO_4^{3-} \cdot 4H^+$	$PO_4^{3-} \cdot 4H^+$	$FeO_4^{2-} \cdot 4H^+$	$SO_4^{2-} \cdot 4H^+$	$CrO_4^{2-} \cdot 4H^+$
R calc.	1.766	1.744	1.661	1.66	1.690	1.581	1.609	1.57	1.607
$r_M + r_O$ [28]	1.76	1.74	1.61	1.68	1.705	1.520	1.600	1.47	1.610
exp.	1.76[a]	1.745[b]	1.638[c]	1.70[d]	1.71[e]	1.53[f]	—	1.50[g]	1.605[g]
q_M	2.375	2.132	2.449	2.137	2.151	2.39	1.806	2.060	1.855
q_O	− 1.594	− 1.533	− 1.612	− 1.284	− 1.288	− 1.348	− 0.951	− 1.015	− 0.964
M–O bond order	0.663	0.782	0.711	1.005	1.060	1.022	1.159	1.13	1.339
K_{z1} calc.	296,850	302,820	302,000	395,300	409,725	373,750	383,000	288,000	500,250
exp.	266,973	—	318,356	295,460	323,821	417,591	319,134	458,619	339,693
ν_{z1} calc.	791	799	798	913	929	887	898	779	1027
exp.	750	—	819	789	826	938	820	983	846
E_{cov} (a.u.)	1.063	1.147	1.142	1.415	1.802	1.674	1.634	2.254	2.312

[a] Ref. (29), data for Ba_3CrO_5 and Ba_2CrO_4.

[b] U. Shigekazu, U. Kazuyori, and K. Keiichi, *Semento Gijetsu Nenpo*, **29,** 32 (1975), data for Ca_2GeO_4.

[c] J. R. Smyth and R.M. Hazen, *Am. Miner.* **58,** 588 (1973), data for Mg_2SiO_4.

[d] Ref. (8), data for $Ba_5(MnO_4)_3Cl$.

[e] E. Banks, M. Greenblatt, and B. Post, *Inorg. Chem.* **9,** 2259 (1970), data for $Ca_2(VO_4)Cl$.

[f] P. E. Mackie, J. C. Elliot, and R. A. Young, *Acta Crystallogr. B* **28,** 1840 (1972), data for $Ca_5(PO_4)_3Cl$. M. Greenblatt, E. Banks, and B. Post, *Acta Cryst. B* **23,** 166 (1967), *Acta Crystallogr. B* **25,** 2170 (1969), data for Ca_2PO_4Cl (and Ca_2CrO_4Cl).

[g] R. W. G. Wyckoff, "Crystal Structures, Second edition," Vol. 3. Interscience, New York, 1960.

used without change in lower symmetry calculations in order to trace the effect of angular distortions of C_{3v}, D_{2d}, and C_s symmetry on the $^3A_2(e^2)$ ground state energy. State energies originating from the d^2 configuration (triplets: $^3A_2$, $^3T_2$, $_a{}^3T_1$, $_b{}^3T_1$ and lowest singlet states: ^1E, $^1A_1$) were calculated by CI using a common set of molecular orbitals obtained by averaging the second-order density matrix in corresponding MCSCF runs over all CSF (10 for triplets, 15 for singlets). In addition, CASSCF calculations have been performed using an $(2e\,4t_2)^2$ active space. With $^3A_2$ and $^3T_2$ being the only symmetry species for triplets this corresponds to simple HF-SCF calculations. State energies [$^3A_2(e^2)$ taken as reference] and energy components are listed and compared with experimental data in Table 4. The MCSCF process did not always converge, especially when electronic states became close in energy. Corresponding fields are left empty in Table 4. In order to analyze the nephelauxetic effect, i.e., the reduction of interelectronic repulsion terms compared to the free ion values, Coulomb (J) and exchange (K) integrals were calculated using frozen orbitals that had been obtained from state averaging over triplet states. Energies of ligand-to-metal charge transfer transitions for tetra-oxo and tetra-hydroxo clusters of Cr^{IV}, Mn^{V}, and Fe^{VI} are obtained using CI, $^3A_2$ HF-SCF orbitals, and an $[1e\,2e]^6$ active space for the $^3A_2(e^2)$ state and orbitals resulting from averaging the second-order density matrix (MCSCF runs) over $3t_2(L) \Rightarrow 2e(3d)$ and $1t_1(L) \Rightarrow 2e(3d)$ charge transfer excitations (active spaces $[3t_2(L)2e(3d)]^8$ and $[1t_1(L)2e(3d)]^8$, respectively) for metal-to-ligand charge transfer states. Transition energies are listed and compared with experimental band maxima positions from literature (17) in Table 5. In order to study the effect of charge transfer states on multiplets of d^2 type we have performed comparative CASSCF calculations extending the active spaces from $[2e(3d)]^2$ to $[1e(L)2e(3d)]^6$ (for the $^3A_2$, ^1E, and $^1A_1$ states) and from $[2e(3d)\,4t_2(3d)]^2$ to $[3t_2(L)2e(3d)4t_2(3d)]^8$ (for the $^3A_2$,$^3T_2$, $_{a,b}{}^3T_1$ states). The results are listed in Tables 6 and 7, respectively.

III. RESULTS AND DISCUSSION

III.1. Results for the Free Ions Cr^{IV}, Mn^{V}, and Fe^{VI}

The d^2 configuration gives rise to ^3F, ^3P, and ^1G, ^1D, and ^1S states whose energy separation, described by the well-known Slater–Condon–Shortley (SCS) theory, is given in terms of two interelectronic replusion parameters, B and C, while a third parameter, A, contributes by $2A$ to shift all multiples by the same energy. We were able to calculate A, B, and C for Cr^{IV}, Mn^{V}, and Fe^{VI} in the following way. Keeping in mind that the independent particle model is more suitable for states with higher spin-multiplicity, we concentrate on the ^3P and ^3F states only and use a common set of SCF orbitals (average of ^3F and ^3P triplets) to calculate Coulomb (J) and exchange (K) integrals for d electrons. These depend on the basis reference chosen. Two combinations of J and K, however, remain invariant under basis transformations:

$$J = \sum_{i,j=1}^{5} J_{ij} = \sum_{i=1}^{5} J_{ii} + 2\sum_{i<j} J_{ij} = 25A + 35C \qquad [2]$$

$$X = \sum_{i,j=1}^{5} K_{ij} = \sum_{i=1}^{5} J_{ii} + 2\sum_{i<j} K_{ij} = 5A + 70B + 35C. \qquad [3]$$

In the SCS theory, the energy difference ΔE between ^3P and ^3F stems entirely from the difference in the corresponding open shell repulsions:

$$\Delta E = E(^3P) - E(^3F) = 15B. \qquad [4]$$

Values of J, X, and ΔE for Cr^{IV}, Mn^{V}, and Fe^{VI} are compiled in Table 1. They are used in combination with Eqs. [2]–[4] to calculate A, B, and C. Compared to values deduced semiempirically from spectral data, our model generally overestimates the B and C parameters in a quite uniform way: B is between 21% (Fe^{VI}) and 25% (Cr^{IV}) too large, and C between 9 (Fe^{VI}) and 13% (Cr^{IV}) too large. This is not surprising because B and C have been derived from HF results which do not take account of correlation with $3s$ and $3p$ electrons.

III.2. Orbital and Bonding Schemes and Valence Stabilization of Cr^{IV}, Mn^{V}, and Fe^{VI} in Tetrahedral Oxo Coordination

Valence orbital energies from $^3A_2(e^2)$ HF-SCF calculations in tetrahedral oxo and hydroxo clusters with Cr^{IV}, Mn^{V}, and Fe^{VI} as obtained from geometry optimizations using TZV basis sets are listed in Table 2 and plotted in Fig. 2. $^3A_2(e^2)$ electronic ground states have been found for all cases except $Fe(OH)_4{}^{2+}$ (see below). Optimized values of the M–O bond lengths (R_{M-O}), $CrO_4{}^{4-} \cdot 4H^+$: 1.766 Å, $MnO_4{}^{3-} \cdot 4H^+$: 1.66 Å, and $FeO_4{}^{2-} \cdot 4H^+$: 1.609 Å, are rather close to those obtained as sums of ionic radii (28) (1.76, 1.68, and 1.60 Å, respectively) and also to M–O bond lengths reported for some Cr^{IV}- and Mn^{V}-containing stoichiometric phases (Ba_3CrO_5 : 1.769 (29) and $Ba_5(MnO_4)_3Cl$: 1.694–1.702 Å (8)). M–O bond lengths for hydroxo clusters are calculated to be slightly lower than those for oxo anions for Cr^{IV} and Mn^{V}($Cr(OH)_4$: 1.73 Å and $Mn(OH)_4{}^+$: 1.628 Å) and larger for Fe^{VI} ($Fe(OH)_4{}^{2+}$: 1.623 Å). The MO scheme obtained is essentially the well-known textbook pattern for transition metal ions in tetrahedral coordination (30) with the typical level ordering

TABLE 4

Energies of Triplet and Selected Singlet Ligand Field Excited States (Relative to $^3A_2$, in cm^{-1}) for Cr^{IV}, Mn^V, and Fe^{VI} in Tetrahedral Hydroxo and Oxo Clusters Obtained by CI (Using $[Av(t_2^{6/5}e^{4/5})]$ Orbitals for Triplet and Singlet States, Respectively) and CASSCF (Using $[2e4t_2]^2$ Active Spaces, in Parentheses) and *d–d* Transitions in Tetrahedral MO_4^z Clusters (M, $z = Cr^{IV}, -4$; $Mn^V, -3$; $Fe^{VI}, -2$) as Obtained from Interpretations of Optical and Near IR Spectral Data[a]

State (first-order crystal field expression) Basis:	$Cr(OH)_4$		$CrO_4^{4-} \cdot 4H^+$		$Mn(OH)_4^+$		$MnO_4^{3-} \cdot 4H^+$		$Fe(OH)_4$		$FeO_4^{2-} \cdot 4H^+$	
	3-21G	TZV	3-21G	TZV	3-21G	TZV	3-21G	TZV	3-21G	TZV	3-21G	TZV
$^3T_2(e^1t_2^1)$	7498	7259	7797	9363	8275	18,321	14,629	13,022	1453	− 251	18,153	15,031
$[10Dq]$	(8077)	(7867)	(9376)	(10,176)	(9203)	(8981)	(16,904)	(15,150)	(6307)	(—)	(22,968)	(19,849)
Exp	9100	9100	9100	9100	10,500	10,500	10,500	10,500	13,000	13,000	13,000	13,000
$_a{}^3T_1(e^1t_2^1)$	12,798	12,433	13,537	15,413	14,013	26,707	21,213	19,690	6990	5169	23,516	20,635
$[10Dq + 12B]$	(13,350)	(13,004)	(15,044)	(—)	(14,941)	(14,622)	(23,606)	(—)	(12,110)	(—)	(28,502)	(—)
Exp	13,900	13,900	13,900	13,900	14,233	14,233	14,233	14,233	17,700	17,700	17,700	17,700
$_b{}^3T_1(t_2^2)$	24,035	24,122	23,075	26,601	24,800	44,345	34,348	32,035	(—)	14,872	40,536	35,560
$[20Dq + 3B]$	(24,550)	(24,644)	(24,231)	(—)	(25,726)	(25,469)	(36,398)	(—)	(—)	(—)	(45,089)	(—)
Exp	20,500	20,500	20,500	20,500	20,600	20,600	20,600	20,600	—	—	—	—
$^1E(e^2)$	13,546	14,118	15,002	14,497	10,724	12,596	12,927	13,008	4974	4894	10,205	10,274
$[8B + 2C]$	(13,931)	(14,500)	(14,541)	(14,033)	(11,162)	(11,965)	(14,146)	(14,303)	(3829)	(3619)	(13,744)	(13,854)
Exp	—	—	—	—	8500	8500	8500	8500	6210	6210	6210	6210
$^1A_1(e^2)$	21,796	22,554	23,306	23,607	17,665	19,762	22,286	22,040	8510	8385	18,090	17,801
$[16B + 4C]$	(22,080)	(16,938)	(24,160)	(—)	(17,433)	(18,524)	(23,309)	(—)	(7062)	(6769)	(21,089)	(—)
Exp	14,730	14,730	14,730	14,730	13,500	13,500	13,500	13,500	9118	9118	9118	9118

[a] All energies are in cm^{-1}. Transition energies are obtained by averaging over split components due to low-symmetric distortions. Experimental data refer to Cr^{IV}: Ca_2GeO_4 (4), Mn^V: $Ca_2(VO_4)Cl$ (21), and Fe^{VI}: K_2CrO_4 (12). Values of B, deduced from experimental data, are: 540 cm^{-1} (Cr^{IV}), 430 cm^{-1} (Mn^V), and 375 cm^{-1} (Fe^{VI}).

TABLE 5
Energies of $^3A_2(e^2)$ and Ligand-to-Metal Charge Transfer States (in cm^{-1}) as Obtained by CI (3-21G basis) and Energies of Band Maxima from Charge Transfer Spectra

Electronic state	Dominant configuration	HF-SCF orbitals	CI active space	$Cr(OH)_4$	$CrO_4^{4-}\cdot 4H^+$	$Mn(OH)_4^{1+}$	$MnO_3^{3-}\cdot 4H^+$	$Fe(OH)_4^{2+}$	$FeO_4^{2-}\cdot 4H^+$
$^3A_2$	$2e^2$	$^3A_2(e^2)$	$[1e2e]^6$	0	0	0	0	0	0
$^3T_2$	$1t_1{}^5 2e^3$	$Av(1t_1{}^{24/5}2e^{16/5})$	$[1t_1 2e]^8$	45,230	49,042	16,828	27,260	− 14,825	6668
$^3T_1$	$1t_1{}^5 2e^3$	$Av(1t_1{}^{24/5}2e^{16/5})$	$[1t_1 2e]^8$	48,019	51,590	22,488	32,652	− 14,711	8329
$^3T_2$	$3t_2{}^5 2e^3$	$Av(1t_2{}^{24/5}2e^{16/5})$	$[3t_2 2e]^8$	57,567	63,639	34,342	49,325	6728	27,968
$^3T_1$	$3t_2{}^5 2e^3$	$Av(1t_2{}^{24/5}2e^{16/5})$	$[3t_2 2e]^8$	60,110	64,073	41,743	50,377	16,671	40,356
ΔE_{CT}[a]				35,000 43,000			32,000		20,000

[a] Taken from Ref. (17) and references cited therein.

TABLE 6
Transition Energies (3-21G basis) within the e^2 ($3d$) Configuration before and after Accounting for Configurational Mixing with Ligand-to-Metal $1e^3 2e^3$ and $1e^2 2e^4$ Charge Transfer States

Cluster	Method	$\Delta E(^3A_2 \Rightarrow {}^1E)$	$\Delta E(^3A_2 \Rightarrow {}^1A_1)$
$Cr(OH)_4$	HF-SCF	14,638	27,651
	CASSCF $[1e(L)2e(3d)]^6$	13,847	24,283
$Mn(OH)_4^{1+}$	HF-SCF	11,697	20,322
	CASSCF $[1e(L)2e(3d)]^6$	6847	11,083
$Fe(OH)_4^{2+}$	HF-SCF	4126	8208
	CASSCF $[1e(L)2e(3d)]^6$	3094	5750

(but note that $2t_2 < 2a_1$ for Mn^V and $FeO_4^{2-}\cdot 4H^+$):

$$1a_1 < 1t_2 < 2a_1 < 2t_2 < 1e < 3t_2 < 1t_1 < 2e < 4t_2. \quad [5]$$

$3t_2$ and $1t_1$ are essentially nonbonding, while $2t_2$ and $1e$ ($\sigma + \pi$ and π type, respectively) are bonding. The energy differences $\Delta E(1t_1 - 1e)$ and $\Delta E(1t_1 - 2t_2)$ (Table 2) reflect stabilizations due to metal–ligand bonding interactions. Ionic contributions to the $1t_1$ and $1e$, $2t_2$ orbital energies are almost completely canceled out (see the discussion of Eq. [13]). The orbital energy difference $\Delta E(2e - 1t_1)$ correlates with the lowest L to M charge transfer transition and is affected by both ionicity and ligand–ligand coupling, leading to an increase and decrease of $\Delta E(2e - 1t_1)$, respectively. As can be seen from Table 2 and Fig. 2, $\Delta E(2e - 1t_1)$ is shifted toward lower energies in the order Cr^{IV}, Mn^V, and Fe^{VI} in agreement with published spectral data, which show a red shift of the charge transfer band in the same direction (4). Going from hydroxo to oxo clusters we notice a small increase of $\Delta E(2e - 1t_1)$ for Cr^{IV} (2700 cm^{-1}), a considerably larger increase for Mn^V (8977 cm^{-1}), and a very large increase for Fe^{VI}(25,767 cm^{-1}). In $Fe(OH)_4^{2+}$, $2e$ and $1t_1$ are very close in energy, whereas they are well separated in $FeO_4^{2-}\cdot 4H^+$ (Table 2). Our results show that terms originating from the $1t_1{}^6 2e^2$ and $1t_1{}^5 2e^3$ configurations follow trends in $1t_1$ and $2e$: thus $^3A_2(2e^2)$ is the ground state for Cr^{IV}, Mn^V, and $FeO_4^{2-}\cdot 4H^+$, but not for $Fe(OH)_4^{2+}$. In the latter case, $^3T_2(e^1 t_2{}^1)$ is found to concur with closely lying states of ligand to metal charge transfer type as possible ground states (see Section III.4.1). An inspection of the orbital contributions in Table 2 shows that the metal orbital

TABLE 7
***d–d* Transition Energies for Triplet States (in cm^{-1}) for $Cr(OH)_4$ and $Mn(OH)_4^+$ Model Clusters as Calculated Using CASSCF (3-21G basis) and Two Different Active Spaces, d^2 $[2e(3d)4t_2(3d)]^2$ and $[3t_2(L)2e(3d)4t_2(3d)]^8$, Illustrating the Effect of Ligand-to-metal Charge Transfer States on e^2, $e^1 t_2{}^1$, and $t_2{}^2$ Triplet States: Energy Expressions (Neglecting Configuration Mixing between $_a{}^3T_1$ and $_b{}^3T_1$) Allowing for Different B Values (Jørgensen Model), B_{ee} (for e^2), B_{et} (for $e^1 t_2{}^1$), B_{tt} (for $e^1 t_2{}^1$) Are Also Given**

Cluster	$Cr(OH)_4$		$Mn(OH)_4^{1+}$		Energy expression (Jørgensen model)
Active space	$[e(3d)t_2(3d)]^2$	$[t_2(L)e(3d)t_2(3d)]^8$	$[e(3d)t_2(3d)]^2$	$[t_2(L)e(3d)t_2(3d)]^8$	
$^3A_2 \Rightarrow {}^3T_2$	8077	10,910	8275	15,828	$10Dq + 8(B_{ee} - B_{et})$
$^3A_2 \Rightarrow {}_a{}^3T_1$	13,351	17,474	14,013	12,706	$10Dq + 4B_{et} + 8B_{ee}$
$^3A_2 \Rightarrow {}_b{}^3T_1$	24,553	27,132	24,800	19,549	$20Dq - 5B_{tt} + 8B_{ee}$

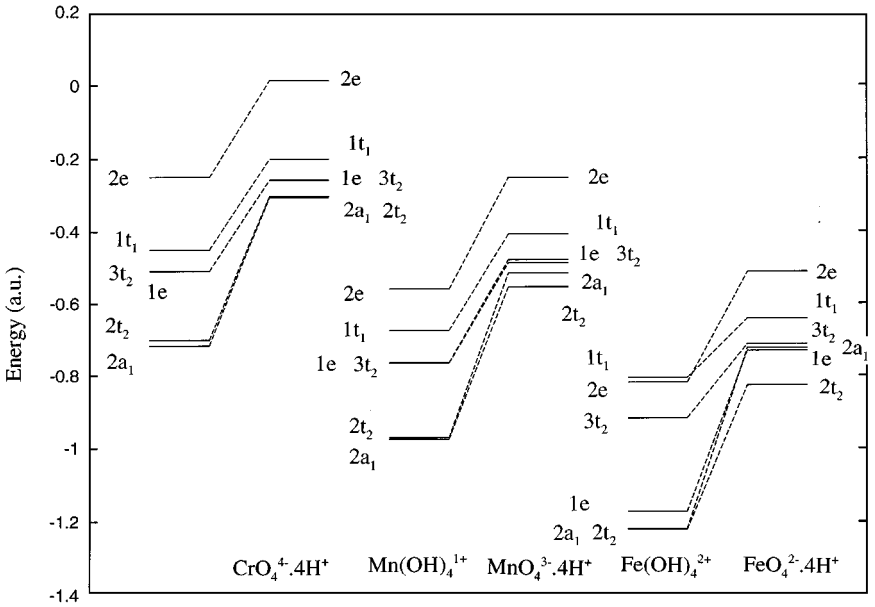

FIG. 2. Orbital energies for hydroxo and oxo model clusters of tetrahedral Cr^{IV}, Mn^{V}, and Fe^{VI}.

percentage in $2e$ decreases from Cr^{IV} to Mn^{V} to Fe^{VI} and from $MO_4 \cdot 4H^+$ to $M(OH)_4$ implying an increase in covalency. Clearly, this is connected with the decrease of $3d(M)$–$2p(O)$ energy separation from Cr^{IV} to Mn^{V} to Fe^{VI} and with the effect of the electrostatic potential due to the charge compensating H^+ ions, which mimics Madelung fields in ionic lattices. It is this field which leads to charge separation in ionic solids. Unfortunately, first principles calculations cannot be used directly to deduce ionic contributions to the metal–ligand bond. In order to study such contributions in a more explicit way, we found the semiempirical approach (18, 31) very useful. If covalency is neglected, the charge distribution within a cluster results from two competing forces, intraatomic and ionic, which tend to reduce and increase charges on different atoms, respectively. Energies needed to produce positively charged particles (ionization potentials) are always larger than those gained when adding electrons to neutral atoms (electronic affinities). Thus, from an atomic point of view, generation of ions is energy consuming in any case. However, the energy loss can be overcompensated by attraction of cations and anions, leading to an increase of electrostatic (Madelung) energy. This is a cooperative effect that is realized in ionic solids. Considering a complex anion $[MO_4]^{m-}$, a transfer of $4q$ electrons from the metal to the ligands produces charges of $-m + 4q$ and $-q$ on the metal and ligand, respectively. With $M = Cr^{IV}$, Mn^{V}, and Fe^{VI} we have $m = 4$, 3, and 2, respectively. In order to estimate the energy needed to transfer $4q$ electrons from the metal to the ligands, Jørgensen introduced the concept of "differential ionization energy,"

$$I(z) = a_0 + a_1 z + a_2 z^2, \qquad [6]$$

which for a given shell and given element M is connected with the ionization energy from M^{n-1} to M^n as

$$I_n = \int_{n-1}^{n} I(z)dz = (a_0 - a_1/2 + a_2/3) + (a_1 - a_2)n + a_2 n^2. \qquad [7]$$

The coefficients a_0, a_1, and a_2 can be calculated by fitting to the successive ionization energies I_1, I_2, and I_3 for a given configuration and are tabulated for the most typical configurations of each atom up to the sixth period (18, 31). Note that $I(z)$ represents the chemical potential of an atom in dependence of its net charge. If one neglects electrostatic forces, the equilibrium charge distribution for the whole cluster $[MO_4]^{m-}$ can be reduced to the equilibrium per bond as given by

$$I_M(-m + kq) = I_O(-q). \qquad [8]$$

Using tabulated values of a_0, a_1, and a_2 for oxygen and M = Cr, Mn, Fe (18, 31), we calculate the charges for M and O to be

$$-0.36, -0.91\ (CrO_4^{4-}), -0.14, -0.72\ (MnO_4^{3-}), \text{ and } 0.17, -0.54\ (FeO_4^{2-}), \qquad [9]$$

predicting small charge separations, as expected in accordance with the electroneutrality principle. Even smaller charges are obtained if metal–ligand overlap (covalency) is taken into account. In order to account for the ionic forces, Madelung energies (E_M) for $[MO_4]^{m-} \cdot 4H^+$ have been calculated as a function of q, using M–O bond lengths (R) as given by sums of the ionic radii, O^{2-}–H^+ distances of 2 Å (see Table 2),

$$\begin{aligned} E_M &= (m_0 + m_1 q + m_2 q^2) R^{-1} \\ m_0 &= [-4m + 3\sqrt{(3/2)}](1+r)^{-1} \\ m_1 &= 4m + 16(1+r)^{-1} - 4r^{-1} \\ &\quad - 6\sqrt{(3/2)}(1 + r + (3/8)r^2)^{-1/2} \\ m_2 &= -16 + 3\sqrt{(3/2)} \\ r &= R_{O-H}/R, \end{aligned} \qquad [10]$$

and Madelung potentials on $M(V_M)$ and $O(V_O)$ given by the expressions

$$\begin{aligned} V_M &= 4[-q + (1+r)^{-1}] \cdot R^{-1} \\ V_O &= \{-m + 4q + (3/2)^{3/2}[-q \\ &\quad + (1 + r + (3/8)r^2)^{-1/2}] + r^{-1}\} \cdot R^{-1}. \end{aligned} \qquad [11]$$

With V_M and V_O the equilibrium condition of $[MO_4]^{m-} \cdot 4H^+$ becomes (compare with Eq. [8])

$$I_M(-m + kq) + V_M = I_O(-q) + V_O. \qquad [12]$$

Using this expression we calculate charges on M and O of 3.82, −1.95 (CrO_4^{4-}), 3.675, −1.67 (MnO_4^{3-}), and 3.40, −1.35 (FeO_4^{2-}). These data, when compared with those from Eq. [9], show the crucial role of ionic bonding for the charge distribution in CrO_4^{4-}, MnO_4^{3-}, and FeO_4^{2-}. The model predicts that charge separation in these species is much larger than claimed by Pauling's electroneutrality principle. More moderate charge separations are obtained from our *ab initio* data and Mulliken population analysis (Table 3). Calculated M and O charges (Cr^{IV}, O: 2.375, −1.594; Mn^{V}, O: 2.137, −1.284; Fe^{VI}, O: 1.806, −0.951) and M–O bond orders (Cr^{IV}–O, 0.663, Mn^{V}–O: 1.005, and Fe^{VI}–O: 1.159) reflect considerable contributions from covalency. In order to get insight into the latter effect we used the orbital energies in Table 2 and took the energy of the nonbonding t_1 as reference to estimate contributions from bonding ($2a_1$, $2t_2$, $1e$) orbitals to the energy of covalent bonding (E_{cov}):

$$E_{cov} = 2\Delta E(1t_1 - 2a_1) + 6\Delta E(1t_1 - 2t_2) + 4\Delta E(1t_1 - 1e). \qquad [13]$$

In Eq. [13], contributions from ligand $2s$ orbitals and ligand–ligand interactions, as well as the doubly occupied $2e$ orbital, are disregarded, the $\Delta E[2e(3d) - 1t_1(L)]$ term being affected considerably by ionicity. The latter is found to play a minor role in Eq. [13], since $1t_1$, $2a_1$, $2t_2$, $3t_2$, and $1e$ (being mostly of ligand type) undergo uniform shifts which cancel in ΔE.

Values of E_{cov} (Table 8, calculated from Eq. [13] and the data in Table 2) increase from Cr^{IV} to Mn^{V} and Fe^{VI} in line with corresponding M–O bond orders (Table 3). Madelung energies (calculated using Eq. [10] and two different charge distributions—formal charges and *ab initio* values, Table 8) show the opposite trend.

The stabilizations of the bonding orbitals $1e$, $2t_2$, and $2a_1$ with respect to $1t_1$, $\Delta E(1t_1 - 1e)$, $\Delta E(1t_1 - 2t_2)$, and $\Delta E(1t_1 - 2a_1)$, can be decomposed into π and σ parts ($3t_2$ is almost nonbonding):

$$\begin{aligned} \Delta E(1t_1 - 1e) &= 8/3\ \pi(3d) \\ \Delta E(1t_1 - 2t_2) &= 8/9\ [\pi(3d) + 3\pi(4p)] \\ &\quad + (4/3)[\sigma(3d) + \sigma(4p)] \\ \Delta E(1t_1 - 2a_1) &= 4\sigma(4s). \end{aligned} \qquad [14]$$

If we neglect contributions from $4p$ orbitals, which are much weaker than those from $3d, 4s$ orbitals, $\pi(3d)$, $\sigma(3d)$ are given by the following expressions:

$$\begin{aligned} \pi_L &= (3/8)\Delta E(t_1 - 1e) \\ \sigma_L &= (3/4)[\Delta E(t_1 - 2t_2) - (1/3)\Delta E(t_1 - 1e)], \\ \text{and} \quad \sigma(4s) &= 1/4\Delta E(t_1 - 2a_1). \end{aligned} \qquad [15]$$

Values for π_L $(3d)$, σ_L $(3d)$, and π_L/σ_L (Table 2) show that π_L, σ_L, and π_L/σ_L increase in the order Cr^{IV}, Mn^{V}, and Fe^{VI} and are larger for OH^- than for O^{2-}.

Ligand–ligand interactions were found to modify orbital level schemes in solids significantly (32). If one restricts to $2p$ orbitals on oxygen and excludes metal–ligand coupling, the

TABLE 8

Atomic Charges from *ab Initio* Calculations and the Ionic Model by Jørgensen (in Parentheses) on Model Clusters $MO_4^z \cdot 4H^+$, and Ionic and Overlap Components of the Bonding Energy (eV)

Cluster	$CrO_4^{4-} \cdot 4H^+$	$MnO_4^{3-} \cdot 4H^+$	$FeO_4^{2-} \cdot 4H^+$
q_M	2.375 (3.82)	2.137 (3.675)	1.806 (3.40)
q_O	−1.594 (−1.95)	−1.284 (−1.67)	−0.951 (−1.35)
E_{mad}	−7.084 (−12.78)	−5.576 (−11.302)	−3.683 (−8.873)
E_{cov}	28.93	38.50	44.47

following orbital energies result:

$$\begin{aligned}
\varepsilon[a_1(L)] &= H_{2p} - 2|V_{pp\sigma}| - |V_{pp\pi}| \\
\varepsilon[e(L)] &= H_{2p} - (1/2)|V_{pp\sigma}| + (1/2)|V_{pp\pi}| \\
\varepsilon[t_2(L,\sigma)] &= H_{2p} + (2/3)|V_{pp\sigma}| + (1/3)|V_{pp\pi}| \\
\varepsilon[t_2(L,\pi)] &= H_{2p} - (1/6)|V_{pp\sigma}| - (11/6)|V_{pp\pi}| \\
\varepsilon[t_1(L)] &= H_{2p} + (1/2)|V_{pp\sigma}| + (3/2)|V_{pp\pi}|.
\end{aligned} \qquad [16]$$

Matrix elements of ligand–ligand covalent mixing of σ and π type, $V_{pp\sigma}$ and $V_{pp\pi}$, respectively, estimated as given by Harrison (33) are used to calculate the orbital energies (Eq. [16]) adopting O–O distances as controlled by M–O separations for $M = Cr^{IV}$, Mn^{V}, and Fe^{VI} (Fig. 3). Since ligand orbitals are doubly occupied, bonding contributions [due to $a_1(L)$, $e(L)$, and $t_2(L,\pi)$] are cancelled by antibonding ones [due to $t_2(L,\sigma)$ and $t_1(L)$]; ligand–ligand coupling does not produce a net bonding effect. The only influence of interligand interactions concerns the energy separation between the ligand $t_2(L,\sigma)$, $t_1(L)$ and metal $3d$ orbitals. It is this difference which governs the ligand-to-metal charge transfer transition (see above). Since metal–ligand distances decrease in the order Cr^{IV}, Mn^{V}, Fe^{VI} (O–O distances become shorter), ligand–ligand interactions become stronger when moving from Cr^{IV} to Mn^{V} and Fe^{VI}, thus contributing (in addition to the drop of H_{3d}–H_{2p} energy) to experimentally observed red shifts of (ligand to metal) charge transfer bands. Since charge transfer gaps are found to be closely related to the stability of the Cr^{IV}, Mn^{V}, and Fe^{VI} valence forms, it follows that ligand–ligand coupling is rather important.

We also have studied the dependence of the ground state energy on structural distortions corresponding to changes in the M–O bond distances (without altering the symmetry) and bond angles leading to a lowering of the symmetry from tetrahedral (T_d) to trigonal (C_{3v}) and tetragonal (D_{2d}). Specifically, the angular distortion parameters 2θ and θ' are defined as being the two O–M–O bond angles along the S_4 axis in the case of D_{2d} symmetry, and the three O–M–O angles along the molecular C_3 axis for C_{3v} symmetry, respectively. Energy plots for the $^3A_2(e^2)$ state versus changes in the M–O bond length and the tetragonal (2θ) and trigonal (θ') angles are depicted in Figs. 4a, 4b, and 4c, respectively. In all cases the curves show minima for tetrahedral geometries. It follows that distortions toward lower symmetries, as reflected by the optical spectra of CrO_4^{4-} (4) and MnO_4^{3-} (34) in various host lattices, are solely due to packing and crystal surrounding effects. A decomposition of the total energy E_t into electron–electron (V_{ee}), nuclear–nuclear (V_{nn}), electron–nuclear (V_{en}), and kinetic energy (T) terms for angular distortions of D_{2d}, and C_{3v} symmetry (Figs. 4b, and 4c) shows that V_{en}, V_{ee}, and V_{nn} are mostly affected by variations in 2θ and θ'. A lowering in symmetry leads to a gain in electron–nuclear attraction energy V_{en}, while the repulsive forces V_{ee} and V_{nn} show the opposite trend, and compensate with a small excess the effect of V_{en}. This leads to absolute minima at T_d. Analogous plots are obtained when discussing lower symmetric distortions of C_s type. In a similar way, the repulsive forces V_{ee} and

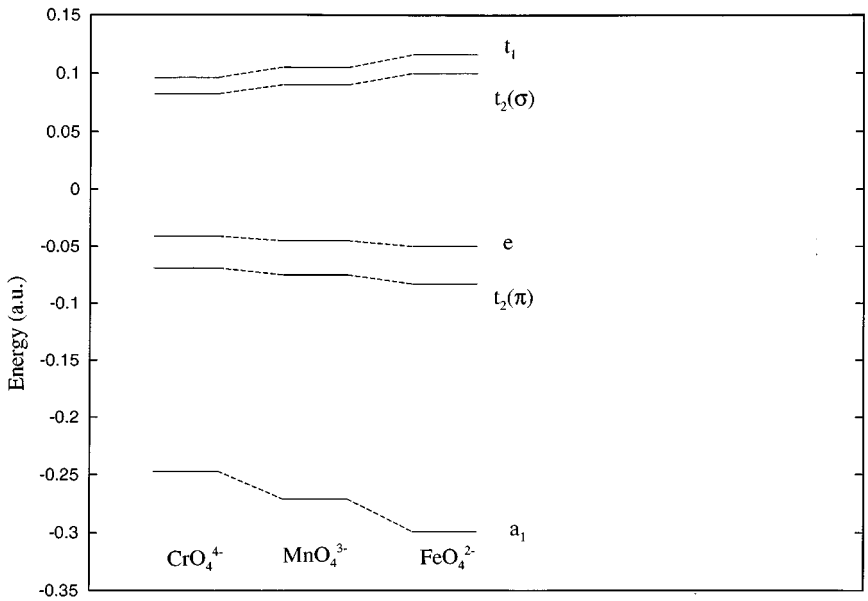

FIG. 3. Orbital levels resulting from ligand–ligand overlap in tetrahedral CrO_4^{4-}, MnO_4^{3-}, and FeO_4^{2-} clusters, calculated using the method of Harrison (33) and O–O separations as controlled by the M–O bond distances [taken as sums of ionic radii from literature, Ref. (28)].

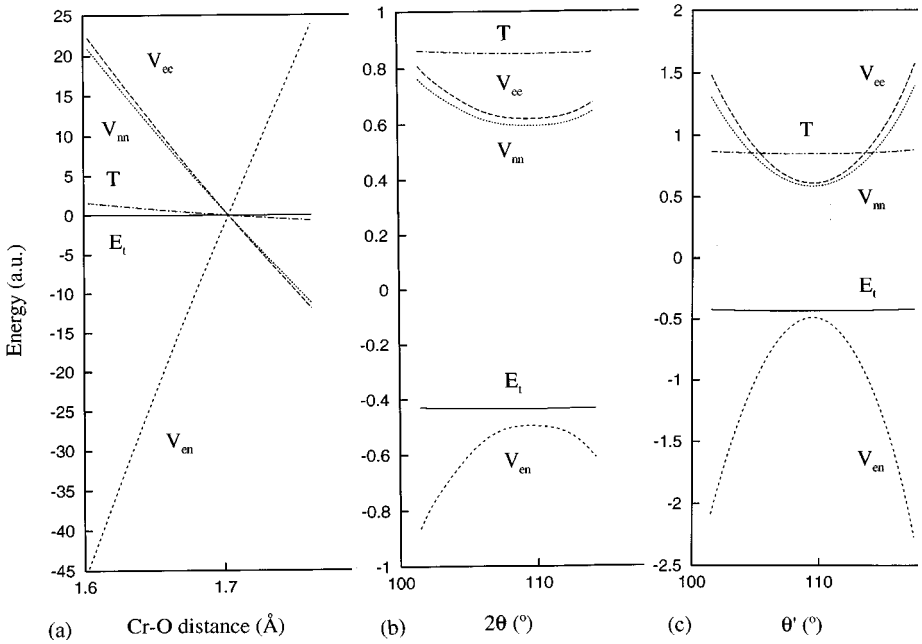

FIG. 4. HF-SCF $^3A_2$ ground state energies and their components (with respect to their values for the tetrahedral equilibrium geometry) for $Cr(OH)_4$ (TZV basis) vs the (a) Cr–O bond distance, (b) tetragonal (2θ), and (c) trigonal (θ') distortion angles. Notations: E_t, total energy; T, kinetic energy; V_{ee}, electron–electron, V_{nn}, nuclear–nuclear, and V_{en}, electron–nuclear potential energies.

V_{nn} are well balanced by the attractive force V_{en} at a distance close to the M–O equilibrium (Fig. 4a). A shortening of the M–O bond is tolerated by the V_{en} term, while V_{ee} and V_{nn} at the same time become less favored. In Fig. 4 we emphasize the important role of repulsive forces (V_{ee} and V_{nn}) when considering configurational changes on the basis of potential energy surfaces and underlying vibronic models. Such contributions are frequently neglected when treating vibronic problems, discussions usually being restricted to one-electronic operators and matrix elements (vibronic constants) (35).

III.3. Valence Stabilization and Mixed Crystal Chemistry of Cr^{IV}, Mn^{V}, and Fe^{VI} in Oxidic Solids

One may ask to what extent the results in Section III.2 can be applied to solids and how incorporation of Cr^{IV}, Mn^{V}, and Fe^{VI} into the tetrahedral sites of oxide hosts can be controlled. We have shown that ionic forces play an important role in stabilizing Cr^{IV}, Mn^{V}, and Fe^{VI} valence species in clusters and the question arises of how Madelung and metal–ligand overlap energies, as well as packing in crystals, can further contribute to this effect.

The isomorphic replacement of host matrix ions (B) by isovalent guest ions (M) leading to solid solutions of the type $A_2M_xB_{1-x}O_4$ is governed by the change in the Gibbs free energy

$$\Delta G(x, T) = \Delta H(x) - T\Delta S(x), \qquad [17]$$

with $\Delta H(x)$ and $\Delta S(x)$ being the mixing enthalpy and entropy given by

$$\Delta H(x) = H(x) - xH_M - (1-x)H_B, \qquad [18]$$

$$\Delta S(x) = -k[x\ln x + (1-x)\ln(1-x)]. \qquad [19]$$

$H(x)$, H_M, and H_B are the enthalpies of $A_2M_xB_{1-x}O_4$, A_2MO_4, and A_2BO_4, respectively. For mixed crystals of $A_3(MO_4)_x(BO_4)_{3-x}Cl$ type, Eqs. [18] and [19] have to be modified correspondingly. According to Eqs. [17], and [19] (with $\Delta S(x)$ being always positive and reaching a maximum at $x = 0.5$), isomorphic mixing is tolerated by entropy because it increases the disorder in the system. In the following discussion we concentrate on $\Delta H(x)$.

Theories of isomorphic substitution in ionic lattices relate $\Delta H(x)$ to differences between the metal–ligand bond lengths for guest (M) and host (B) ions, leading to equations of the form (39–43)

$$\Delta H_1(x) = x(1-x)(dR/R_B)^2 H_B$$
$$dR = R_M - R_B. \qquad [20]$$

Equation [20] presupposes that metal–ligand bond distances in a mixed crystal depend on x as

$$R = xR_M + (1-x)R_B = R_B + x \cdot dR, \qquad [21]$$

implying that R is affected in a cooperative way by M and B. Equation [20] was derived for typical ionic solids. H_B is rather complex and contains, besides Madelung terms, contributions from inner shell repulsions, atomic shifts from ideal lattice positions, and/or cationic ordering. Madelung energies and $\Delta H(x)$ values for d^2 ions and various oxide hosts [Cr^{IV}: olivines A_2BO_4, A,B = Mg, Si; Ca, Ge, Mn^V: apatites, $A_5(BO_4)_3Cl$, A, B = Sr, P; Ba, P, and spodiosites $A_2(BO_4)Cl$, A, B = Ca, P; Ca, V; Sr, V, and Fe^{VI}: A_2BO_4, A, B = K, Cr; K, S] have been calculated using the computer program MAPLE (44–46) and Eq. [20]. $\Delta H(x = 0.5)$ are found to be rather small for M and B with similar ionic radii (Cr^{IV}, Ge^{IV}; Mn^V, V^V; and Fe^{VI}, Cr^{VI}) allowing one to expect that Cr^{IV}, Mn^V, and Fe^{VI} may be stabilized in larger concentrations by substituting Ge^{IV}, V^V, and Cr^{VI}, respectively. This is supported by experimental data for which doping of Cr^{IV} and Fe^{VI} to up to 30% (in Ca_2GeO_4 (1)) and 50% (K_2CrO_4 (38)) was reported. In contrast, $\Delta H(x)$ are calculated to be rather large for ions which differ considerably in their radii, such as Cr^{IV} compared to Si^{IV}, Mn^V to P^V, and Fe^{VI} to S^{VI} [e.g., 1770 K ($Mg_2Cr_{0.5}Si_{0.5}O_4$), 15,153 K ($Ba_5(P_{0.5}Mn_{0.5}O_4)_3Cl$), and 674 K ($K_2Fe_{0.5}S_{0.5}O_4$)]. In view of this it is rather surprising that a continuous series of mixed crystals has been reported for $Ba_5(MnO_4)_x(PO_4)_{3-x}Cl$ already at 800 K (8) and for $K_2Fe_{0.5}S_{0.5}O_4$ even at lower temperatures (38). Obviously, the prerequisites of Eq. [20] are not fulfilled for Mn^V and Fe^{VI}. We have shown by means of optical spectroscopy and theoretical analysis (21) that already small amounts of Mn^V in $Ba_5(PO_4)_3Cl$ assume bond lengths of the pure $Ba_5(MnO_4)_3Cl$ compound, in contrast to Eq. [21]. The same observation was also made in doped materials such as Cr^{IV} in Mg_2SiO_4 (37) and Fe^{VI} in K_2SO_4 (12), the smaller cavity of the tetrahedral host sites being manifested only by a slight increase of the cubic ligand field splitting. Using the computer program MAPLE (44–46), space filling percentages for oxide host lattices have been calculated adopting a rigid sphere model and ionic radii from literature (28). Most materials under consideration are calculated not to be very densely packed [olivine, Ca_2GeO_4 (51%), spodiosites $A_2(BO_4)Cl$, A, B: Ca, V (66%), Sr, V (60.1%), apatites $A_5(BO_4)_3Cl$, A, B = Sr, P (62.5%), Ba, P (60.3%), Ba, Mn (56.8%)], the only exceptions being Mg_2SiO_4 (71.3%) and $Ca_2(PO_4)Cl$ (68.7%) (compare with the volume fraction of 74.05% for close packing). The smaller the space occupation, the larger the number of guest ions larger in size than the host ions that can be incorporated. M–O bond orders and values of E_{cov} (calculated as in Eq. [13] but including 2s contributions of oxygen, see Table 3) indicate considerable covalency for all tetrahedral species under consideration.

Contributions to $H(x)$ (Eq. [17]) from covalent bonding, being additive and of short range character, lead to rather small $\Delta H(x)$ values. Considering long range interactions (ionic bonds) cooperative effects Eq. [20] may lead to rather large $\Delta H(x)$ values. Real situations include both effects. Our results clearly show that covalency increases while ionicity decreases in the order Cr^{IV} to Mn^V and Fe^{VI} (see Section III.2). Thus for Mg_2SiO_4 with the largest fraction of occupied volume and a considerable misfit between Cr^{IV} and Si^{IV} ionic radii (about 0.13 Å) ionic forces are expected to be larger, thus tending to increase $\Delta H(x)$ and prevent incorporation of larger amounts of Cr^{IV}. The preference of Cr^{III} for occupying octahedral positions (replacing Mg^{II} ions at octahedral sites with C_s and C_i symmetry) contributes further to this effect. Unfortunately, there are no data on $Cr:Mg_2SiO_4$ with higher concentrations of Cr and its distribution between the tetrahedral (Cr^{IV}) and octahedral (Cr^{III}) positions. For Mn^V and Fe^{VI} covalency prevails and correspondingly higher amounts can be stabilized by doping into tetrahedral sites of smaller host ions such as P^V ($Ba_5(PO_4)_3Cl$) and S^{VI}(K_2SO_4), respectively.

III.4. Excited States

III.4.1. Electronic transitions within the d^2-configuration. In a tetrahedral environment the d^2-configuration spans a series of multiplets,

$$\begin{aligned} {}^3F &\Rightarrow {}^3A_2 + {}^3T_2 + {}^3T_1 \\ {}^3P &\Rightarrow {}^3T_1 \\ {}^1G &\Rightarrow {}^1E + {}^1A_1 + {}^1T_1 + {}^1T_2, \end{aligned} \qquad [22]$$

giving rise to electronic transitions from the ground state ${}^3A_2$ into the ${}^3T_2$, ${}_a{}^3T_1$, ${}_b{}^3T_1$, ${}^1E$, and ${}^1A_1$ excited states.[3] These correspond to absorption maxima in the optical and near IR spectra which usually are split into sublevels due to low symmetric distortions. In interpretations of the optical and near IR spectra of these ions it is tacitly assumed that the d^2 configuration remains well defined for $CrO_4{}^{4-}$, $MnO_4{}^{3-}$, and $FeO_4{}^{2-}$. In Table 4 we list transition energies from experiment [averaged over the low-symmetric splittings which are not interesting in the context here, but see Ref. (21)] as well as first-order crystal field expressions and B and $10Dq$ parameter values. In Table 4 we also present calculations on $M(OH)_4{}^z$ and $MO_4{}^{z'}$ model clusters (M, z, $z' = Cr^{4+}$, 0, −4; Mn^{5+}, 1, −3; Fe^{6+}, 2, −2) using HF-SCF [$Av(t_2{}^{6/5}e^{4/5})$] and CASSCF adopting different

[3] Only the lowest lying ${}^1E$ and ${}^1A_1$ states will be discussed here, the effect of higher ones being explicitly taken into account via CI and CASSCF.

basis sets (3-21G and TZV). For CASSCF convergence was not always achieved; corresponding fields are left blank in Table 4. The theoretical values for transitions to triplet states in CrO_4^{4-} are in better agreement with experimental values than $^3A_2 \Rightarrow {}^1E$ and $^3A_2 \Rightarrow {}^1A_1$, calculated about 60% higher in energy. The reason for this is that electronic correlation in the ^1E and $^1A_1$ states is underestimated in the simple $Av(2e, 3t_2)^2$ HF-SCF and even the CASSCF treatments. Transition energies (3-21G basis) have been decomposed into changes due to electron–nuclear (ΔV_{en}), electron–electron (ΔV_{ee}), and kinetic (ΔT) energies. Concerning the $10Dq$ ($^3A_2 \Rightarrow {}^3T_2$) transition energy we note, for hydroxo clusters, that T is the only positive term. This changes when going to $MO_4^{z'}$, in which case ΔV_{en} dominates the sign of $10Dq$. Going from Cr^{IV} to Mn^V and Fe^{VI} clusters we note a drastic deterioration of the agreement between theoretical and experimental transition energies for oxo anions (Table 4). We attribute these changes to extensive mixing of charge transfer states which modifies the simple ligand field picture (see Section III.4.3). When we compare the results for $Fe(OH)_4^{2+}$ with those for $FeO_4^{4-} \cdot 4H^+$, we note once more the important role of Madelung energy in the latter case for the stabilization of Fe in a d^2 valence state. Thus $10Dq$ for $Fe(OH)_4^{2+}$ is calculated to be very small (3-21G) or even negative (TZV). At the same time $^3A_2(e^2)$ and $^3T_2(e^1t_2^1)$ concur with $O \Rightarrow Fe$ charge transfer states as possible ground states in contrast to $FeO_4^{2-} \cdot 4H^+$.

III.4.2. Charge transfer transitions. When attempting to calculate ligand-to-metal charge transfer states for tetrahedral Cr^{IV}, Mn^V, and Fe^{VI} using the CASSCF method we encountered lack of convergence in most cases. Thus calculations using an active space including $3t_2$, $1e$, $1t_1$, and $2e$ orbitals and 18 electrons (3-21G basis and $3t_2^6 1e^4 1t_1^6 2e^2$ reference) were only successful for $Cr(OH)_4$ and $Mn(OH)_4^{1+}$ with lowest charge transfer states at 33,256 cm^{-1} (with 46.5 and 48.8% contributions from the $1t_1(L) \Rightarrow 2e$ and $3t_2(L) \Rightarrow 2e$ charge transfer transitions, respectively) and 8890 cm^{-1} (79% $1t_1(L) \Rightarrow 2e$). They are well separated from the d^2 states for Cr^{IV} but start to overlap with them in the Mn^V case. The results predict $^3A_2(2e^2)$ ground states in both clusters with negligible contributions from other configurations for Cr^{IV} (99.8% $\ldots 2e^2$) but larger for Mn^V (94% $\ldots 2e^2$). In view of the rather restrictive applicability of the CASSCF procedure to active spaces beyond the d^2 manifold we performed less accurate CI calculations based on HF-SCF $^3A_2(e^2)$ orbitals and a $[1e(L)2e(3d)]^6$ active space for $^3A_2(e^2)$ and $Av(1t_1^{24/5}2e^{16/5})$ and $Av(3t_2^{24/5}2e^{16/5})$ frozen orbitals (averages over triplets) as well as $[1t_12e]^8$ and $[3t_22e]^8$ active spaces for the $1t_1 \Rightarrow 2e$ and $3t_2 \Rightarrow 2e$ ligand-to-metal charge transfer states, respectively (Table 5). The lowest energy charge transfer states stem from the $1t_1^5 2e^3$ configuration followed by the $3t_2^5 2e^3$ configuration. The data in Table 5 are rather approximate and compare poorly with experimental charge transfer spectra, but our results clearly demonstrate that energies of charge transfer transitions decrease in the order Cr^{IV}, Mn^V, and Fe^{VI} and from oxo to hydroxo clusters. The CI calculation on $Fe(OH)_4^{2+}$ results in a drop of the $^3T_2(1t_1^5 2e^3)$ state below $^3A_2(1t_1^6 2e^2)$, and at the same time in strong intermixture with the $^3T_2(1t_1^6 2e^1 4t_2^1)$ ligand field state. In contrast to that, the CI calculation of FeO_4^{2-} still gives a $^3A_2(e^2)$ ground state. It is tempting to relate this result, in spite of the inherent approximations, with the fact that FeO_4^{2-} species are stabilized in solids and in cold and concentrated solutions of KOH but become extremely unstable and oxidizing in acidic media. Obviously, electrostatic forces in crystals and concentrated ionic solutions (high-ionic powers) tend to stabilize Fe^{VI} by increasing the energy gap between metal—d^2 and $d^3\underline{L}$ ($\underline{L}$, hole on the ligand) charge transfer states. This result seems to be quite general. The stability of the unusual oxidation states decreasing in the order Cr^{IV}, Mn^V, and Fe^{VI} correlates nicely with the lowest ligand-to-metal charge transfer energy (35,000, 33,000, and 21,000 cm^{-1}, respectively (17)).

III.4.3. Effect of charge transfer states on the d–d transitions. As suggested in (32) and latter demonstrated in (22), ligand field parameterization schemes such as the crystal field and angular overlap model fail when d^n and $d^{n+1}\underline{L}$ charge transfer configurations become strongly intermixed. Decreasing charge transfer energies in the isoelectronic series Cr^{IV}, Mn^V, and Fe^{VI} leads to a violation of the prerequisites of these models which, when applied to transitions within the ground state e^2 configurations, were shown to work quite well for Cr^{IV}, with moderate success for Mn^V, and not to be applicable for Fe^{VI} (22). In order to check this, we performed HF-SCF calculations on the separate $^3A_2$, ^1E, and $^1A_1$ terms from $2e^2$ and compared them with CASSCF results on the same states with an active space of four orbitals [$1e(L)$ and $2e(3d)$] and 6 electrons. Results for Cr^{IV}, Mn^V, and Fe^{VI} are listed in Table 6 and illustrated in Fig. 5. The $^3A_2$ ground state of Cr^{IV} is almost unaltered by charge transfer states ($1e^3 2e^3$) in contrast to Mn^V and Fe^{VI} which are calculated to be shifted by 2063 and 5900 cm^{-1}, respectively, to lower energies:

	$\Delta E(^3A_2)$	$\Delta E(^1E)$	$\Delta E(^1A_1)$
Cr^{IV}	− 307	− 1098	− 3675
Mn^V	− 2063	− 6913	− 11,302
Fe^{VI}	− 5903	− 6935	− 8362

[23]

As seen from [23], the influence of charge transfer states gains importance in the order of increasing term energy from $^3A_2$ to ^1E and $^1A_1$ and becomes increasingly

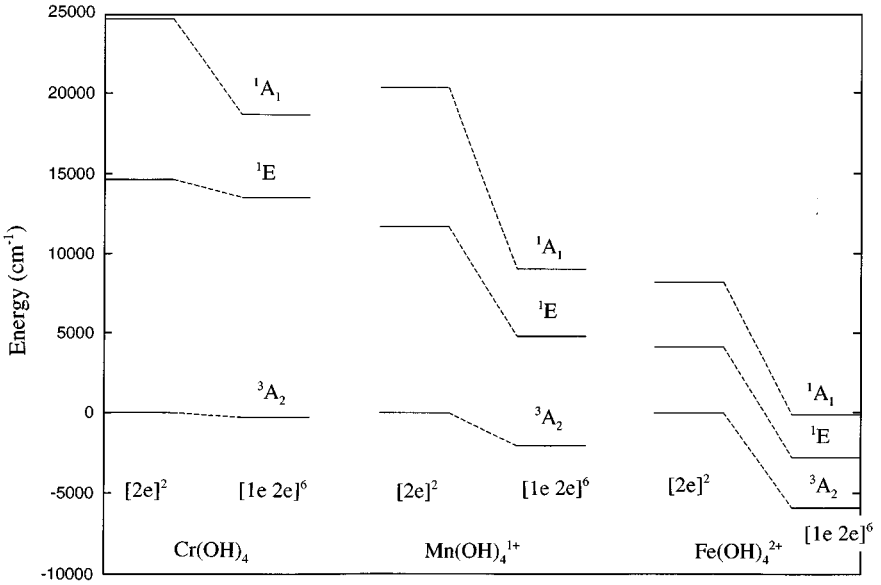

FIG. 5. Energies of states due to the $2e^2$ (d^2) ligand field configuration from HF-SCF and $[1e(L)e]^6$ CASSCF calculations on $Cr(OH)_4$, $Mn(OH)^{1+}$, and $Fe(OH)^{2+}$ model clusters.

pronounced from Cr^{IV} to Mn^{V} and Fe^{VI}, in full accordance with our recent results (22). The larger effect of the $1e^32e^3$ and $1e^22e^4$ configurations on $^1A_1$, followed by ^1E and $^3A_2$ also leads to lower transition energies for $^3A_2 \Rightarrow {}^1E$ and $^3A_2 \Rightarrow {}^1A_1$ compared to their corresponding HF-SCF values.

In the ligand field picture, the energies of $^3A_2 \Rightarrow {}^1E$, and $^3A_2 \Rightarrow {}^1A_1$ are given (to first order) by Coulomb repulsion terms only: $8B + 2C$ (^1E) and $16B + 4C$ ($^1A_1$), respectively (see Table 4). Therefore, one has to allow for reduced values of B and C, which differ among various configurations and even multiplets. The reduction of B and C values in coordinated ions from their values in free gaseous ions, referred to as a nephelauxetic (cloud-expanding) effect has been studied in great detail by Schäffer and Jørgensen (19, 20) and is attributed to two different kinds of covalency. The reduction of B and C stemming from an expansion of the d orbitals caused by a lowering of the cationic charge due to electron transfer from the ligands was called "central field covalency," while the variation of B and C among various configurations which is caused by different overlap between metal and ligand orbitals of e and t_2 symmetry reflects "symmetry restricted covalency." Results from interpretations of the optical spectra of tetrahedral Cr^{IV}, Mn^{V}, and Fe^{VI} are characterized by B values which are in lines with the increasing covalency (see Table 4). A detailed analysis of the optical spectra based on Eq. [1] showed a significant reduction of B and C becoming stronger from $2e^2$ to $2e^14t_2{}^1$ and $4t_2{}^2$ (21). In order to study more closely various contributions to the nephelauxetic effect we have calculated Coulomb $J(i,j)$ and exchange $K(i,j)$ integrals for $M(OH)_4{}^z$ and $MO_4{}^{z'} \cdot 4H^+$ clusters ($M = Cr^{IV}$, Mn^{V}, and Fe^{IV}) adopting, as in ligand field theory, common orbitals [$i,j = d_{x2-y2}$, d_{z2} ($2e$) and d_{xz}, d_{yz}, d_{xy} ($4t_2$) type MO's] for all multiplets obtained using an average of triplet wavefunctions [$Av(2e^{4/5}4t_2{}^{6/5})$]. Coulomb repulsion in a cubic field is fully specified in terms of 10 independent parameters $a, b, \ldots, j$ defined by Griffith (48). Assuming spherical symmetry, these are further expressed in terms of the Racah parameters A, B, and C. Griffith parameters for the free ions (calculated using A, B, and C from Table 1) have been compared with corresponding values in the clusters, yielding reduction factors (β) for various clusters and strong field configurations (Fig. 6). As expected, β are smaller than 100% and shift to lower values from Cr^{IV} to Mn^{V} and Fe^{VI}. However, for a given cluster, they vary in a wide range and do not show the expected lowering when moving from e^2 to $e^1t_2{}^1$ and $t_2{}^2$. Therefore in a treatment restricted to ligand field orbitals only, such as $2e$ and $4t_2$, the trends in B_{ee}, B_{et}, and B_{tt} as given by Eq. [1] with $e > t$ could not be verified. The well-known decrease of β within a given $3d$ subshell when electronic configurations with more localized orbitals are compared with configurations including less localized orbitals (20) can only be reproduced when charge transfer states are taken into account. In Table 7 energies due to transitions within the d^2 shell for $Cr(OH)_4$ and $Mn(OH)_4{}^+$ from CASSCF calculations (3-21G basis, [$2e(3d)$, $4t_2(3d)]^2$) are listed and compared with corresponding CASSCF results obtained using [$3t_2(L)e(3d)4t_2(3d)]^8$ active spaces. Energy expressions allowing for variable B values for the e^2, $e^1t_2{}^1$, and $t_2{}^2$ strong field configurations are also given. In full support of the Jørgensen concept ($B_{ee} > B_{et}$) the

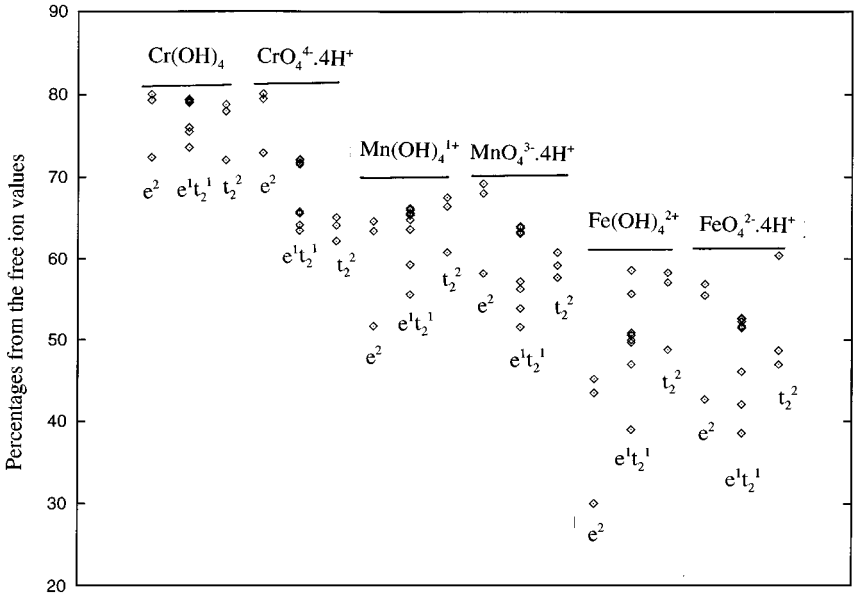

FIG. 6. Nephelauxetic ratios β (percentages from the free ion values) of various Coulomb repulsion integrals of e^2, $e^1t_2{}^1$, and $t_2{}^2$ type for the d^2 Cr^{IV}, Mn^V, and Fe^{VI} ions in tetrahedral hydroxo and oxo model clusters as calculated using molecular orbitals obtained from HF-SCF and averaging over d^2 triplet states $[Av(e^{4/5}t_2{}^{6/5})]$.

$^3A_2 \Rightarrow {}^3T_2$ energy is found to increase switching from d^2 to active spaces involving charge transfer states. As expected, the effect is stronger for Mn^V ($\delta\Delta E = 7553\,cm^{-1}$) then for Cr^{IV} ($\delta\Delta E = 2883\,cm^{-1}$). The effect of charge transfer transitions on $^3A_2 \Rightarrow {}_a{}^3T_1$ and ${}_b{}^3T_1$ is not easy to interpret, for the ${}_a{}^3T_1$ and ${}_b{}^3T_1$ states are already mixed in an ionic model via interelectronic repulsion (6*B*). Our results show, however, that with decreasing charge transfer energies from Cr^{IV} to Mn^V both transitions drop in energy. Thus coupling of d^2 with corresponding $d^3\underline{L}$ charge transfer configurations becomes larger in the order of increasing metal–ligand covalency and decreasing d^2–$d^3\underline{L}$ energy separation—e^2, $e^1t_2{}^1$, and $t_2{}^2$. The use of reduction factors in the way given by Eq. [1] is a useful tool to account for effects beyond the d^2 subshell while still preserving the attractive features of the ligand field approach.

IV. CONCLUSIONS

1. First principle calculations on model clusters of the isoelectronic d^2 cations Cr^{IV}, Mn^V, and Fe^{VI}, tetrahedrally coordinated by OH^- and O^{2-} ligands, supplemented by a semiempirical approach (Jørgensen *et al.*), allow the characterization of the stabilization of these oxidation forms in their $^3A_2(e^2)$ ground states in terms of competing electrostatic (Madelung) and covalent bonding. Covalency tends to reduce charges on *M* and O due to transfer of electrons from the ligand to the metal. Ionic bonding in crystals acts in the opposite direction; it tends to cause charge separation and ionic species with a maximal gain of electrostatic energy. Ionicity is found to decrease in the order Cr^{IV}, Mn^V, and Fe^{VI}, while covalent bond energy increases, accompanied by a decrease of ligand-to-metal charge transfer energies.

For Fe^{VI}, the electrostatic Madelung energy is found to play a crucial role in stabilizing tetrahedral $FeO_4{}^{2-}$ species by counteracting intraatomic forces and covalency, the latter effects tending to alter the oxidation state. Therefore, the $^3A_2(e^2)$ state in $Fe(OH)_4{}^{2-}$ model clusters is found not to be the ground state in contrast to $FeO_4{}^{2-}$ with charge compensating H^+ ions. In accordance with this concept, $FeO_4{}^{2-}$ ions are stabilized in lattices such as K_2SO_4 and K_2CrO_4 and concentrated alkaline solutions of KOH, but become extremely oxidizing in acidic media.

2. Current theories of isomorphic substitution are found not to be applicable for the systems under consideration. The comparison between structural and spectral data shows that Mn^V and Fe^{VI} ions in mixed crystals assume geometries rather close to those known in stoichiometric Mn^V and Fe^{VI} phases. The contributions from covalent bonding for such ions are large enough to overcome the elastic energy needed when replacing smaller host ions with larger ones. Energies from covalent bonding are additive and mixing enthalpies are small or negligible leading to the possibility of continuous solid solutions even when guest and host ions, such as Mn^V, P^V and Fe^{VI}, Cr^{VI}, differ significantly in size.

3. *Ab initio* calculations show that interelectronic repulsion parameters of the tetra-oxo coordinated Cr^{IV}, Mn^V, and Fe^{VI} are significantly reduced from their free ionic

values with the clear trend

$$B(Cr^{IV}) > B(Mn^{V}) > B(Fe^{VI}).$$

This reduction is due partly to central field covalency, and partly to a decrease of B in the order of the strong field configurations e^2, $e^1t_2{}^1$, and $t_2{}^2$ (symmetry restricted covalency). The results allow us to relate the changes in B with the coupling of the d^2 states and the ligand-to-metal charge transfer states. This coupling increases from e^2 to $e^1t_2{}^1$ and $t_2{}^2$, because the energetic separation from charge transfer states decreases in this sequence. The effect becomes increasingly pronounced from Cr^{IV} to Mn^{V} and Fe^{VI} since covalency increases while charge transfer states are shifted toward lower energies in this sequence.

4. The energy decrease of charge transfer states accompanied by an increasing influence on the d^2 multiplets leads to a violation of the prerequisites of the ligand field model. Intermixing is weak for Cr^{IV}, moderate for Mn^{V}, and strong for Fe^{VI}. Ligand field theory is therefore not applicable to Fe^{VI} oxo complexes.

ACKNOWLEDGMENTS

The authors are grateful to the Volkswagenstiftung for a research grant and to Doz. Dr. J. Degen (Institut für Theoretische Chemie, Heinrich-Heine Universität, Düsseldorf) for his kind support and hospitality. Thanks are due to Prof. Dr. D. Reinen (Marburg, Germany) for helpful discussions and encouragement.

REFERENCES

1. D. Reinen, U. Kesper, M. Atanasov, and J. Roos, *Inorg. Chem.* **34,** 184 (1995).
2. M. F. Hazenkamp, U. Oetliker, U. Kesper, D. Reinen, and H. U. Güdel, *Chem. Phys. Lett*. **233,** 466 (1995).
3. M. Atanasov, *Chem. Phys. Lett*. **234,** 313 (1995).
4. M. F. Hazenkamp, H. U. Güdel, M. Atanasov, U. Kesper, and D. Reinen, *Phys. Rev. B.* **53,** 2367 (1996).
5. J. B. Milstein and S. L. Holt, *Inorg. Chem.* **8,** 1021 (1969).
6. J. B. Milstein, J. Ackerman, S. L. Holt, and B. R. McGarvey, *Inorg. Chem.* **11,** 1178 (1972).
7. R. Borromei, L. Oleari, and P. Day, *J. Chem. Soc., Faraday Trans. 2*, **77,** 1563 (1981).
8. D. Reinen, H. Lachwa, and R. Allmann, *Z. Anorg. Allg. Chem.* **542,** 71 (1986).
9. H. Lachwa, and D. Reinen, *Inorg. Chem.* **28,** 1044 (1989).
10. L. di Sipio, G. De Michelis, E. Baiocchi, and G. Ingletto, *Trans. Met. Chem.* **5,** 164 (1980).
11. M. Herren, and H. U. Güdel, *Inorg. Chem.* **31,** 3683 (1992).
12. T. C. Brunold, A. Hauser, and H. U. Güdel, *J. Lumin.* **59,** 321 (1994).
13. V. Petricevic, S. K. Gayen, R. R. Alfano, K. Yamagishi, H. Anzai, and Y. Yamaguchi, *Appl. Phys. Lett*. **52,** 1040 (1988).
14. V. Petricevic, S. K. Gayen, and R. R. Alfano, *Appl. Phys. Lett*. **53,** 2590 (1988).
15. H. R. Verdun, L. M. Thomas, D. M. Andrauskas, T. McCollum, and A. Pinto, *Appl. Phys. Lett*. **53,** 2593 (1988).
16. V. Petricevic, S. K. Gayen, and R. R. Alfano, "OSA Proceedings on Tunable Solid-State Lasers" (M. L. Shand, and H. P. Jenssen, Eds.), Optical Society of America, Washington, DC, 1989.
17. D. Reinen, W. Rauw, U. Kesper, M. Atanasov, H. U. Güdel, M. Hazenkamp, and U. Oetliker *J. Alloys Compounds*, in press.
18. C. K. Jørgensen, S. M. Horner, W. E. Hatfield, and S. Y. Tyree, Jr., *Int. J. Quant. Chem.* **1,** 191 (1967).
19. C. E. Schäffer, and C. K. Jørgensen, *J. Inorg. Nucl. Chem.* **8,** 143 (1958).
20. C. K. Jørgensen, *Progr. Inorg. Chem.* **4,** 73 (1962).
21. M. Atanasov, H. Adamsky, and D. Reinen, *Chem. Phys.* **202,** 155 (1996).
22. M. Atanasov, *Chem. Phys.* **195,** 49 (1995).
23. M. W. Schmidt, K. K. Baldridge, J. A. Boatz, S. T. Elbert, M. S. Gordon, J. H. Jensen, S. Koseki, M. Matsunaga, K. Nguyen, S. J. Su, T. L. Windus, M. Dupuis, and J. A. Montgomery, *J. Comput. Chem.* **14,** 1347 (1993).
24. J. S. Binkley, J. A. Pople, and W. J. Hehre, *J. Am. Chem. Soc*. **102,** 939 (1980).
25. K. D. Dobbs, and W. J. Hehre, *J. Comput. Chem.* **8,** 861 (1987).
26. A. J. H. Wachters, *J. Chem. Phys.* **52,** 1033 (1970).
27. L. G. Vanquickenborne, P. Hoet, and K. Pierloot, *Inorg. Chem.* **25,** 4228 (1986).
28. R. D. Shannon, *Acta Crystallogr.* **A32,** 751 (1976).
29. G. Liu, J. E. Greedan, and W. Gong, *J. Solid. State Chem.* **105,** 78 (1993).
30. C. J. Ballhausen, and H. B. Gray, "Molecular Orbital Theory, An Introductory Lecture Note and Reprint Volume," p. 127. Benjamins, New York Amsterdam, 1965.
31. C. K. Jørgensen, "Modern Aspects of the Ligand-Field Theory." North-Holland, Amsterdam, 1971.
32. G. A. Sawatzky, "Proceedings, Spring College in Condensed Matter on Superconductivity, Trieste," 1992.
33. W. A. Harrison, "Electronic Structure and the Properties of Solids—The Physics of the Chemical Bond." Freeman, San Francisco, 1980.
34. U. Oetliker, M. Herren, H. Güdel, U. Kesper, C. Albrecht, and D. Reinen, *J. Chem. Phys.* **100,** 8656 (1994).
35. I. B. Bersuker, "The Jahn–Teller Effect and Vibronic Interactions in Modern Chemistry." Plenum Press, New York, 1984.
36. I. B. Bersuker, "The Jahn–Teller effect—A Bibliographic Review." Plenum Press, New York, 1984.
37. W. Jia, H. Liu, S. Jaffe, W. M. Yen, and B. Denker, *Phys. Rev. B* **43,** 5234 (1990), and references therein.
38. B. Helferich and K. Lang, *Z. Anorg. Allg. Chem.* **263,** 169 (1950).
39. I. A. Wasastjerna, *Soc. Sci. Fenn., Comment. Phys.-Math* **15**(3), (1949).
40. V. Hovi, *Soc. Sci. Fenn., Comment. Phys.-Math* **15**(12), (1950).
41. J. Hietala, *Ann. Acad. Sci. Fenn., A* **VI** (121), (1963).
42. J. Hietala, *Ann. Acad. Sci. Fenn., A* **VI** (122), (1963).
43. V. S. Urusov, "Theory of Isomorphic Substitution" (in Russian), Nauka, Moscow, 1977.
44. R. Hübenthal, "Program MAPLE," Version 3.03.
45. R. Hoppe, *Angew. Chem.* **78,** 52 (1966).
46. R. Hoppe, S. Voigt, H. Glaum, J. Kissel, H. P. Müller, and K. Bernet, *J. Less-Common Met*. **156,** 105 (1989).
47. K. Nakamoto, "Infrared and Raman Spectra of Inorganic and Coordination Compounds." Wiley, New York, 1978.
48. J. S. Griffith, "The Theory of Transition Metal Ions," Cambridge Univ. Press, London, 1971.